Chemical Kinetics and Diffusion in Poly(butylene Terephthalate) Solid-State Polycondensation: Experiments and Theory

C. GOSTOLI,* F. PILATI,† G. C. SARTI,* and B. DI GIACOMO,† †*Istituto Chimico and* **Istituto di Impianti Chimici, Facoltà di Ingegneria, Università di Bologna, Bologna, Italy*

Synopsis

Postpolymerization was obtained in solid PBT sheets, by annealing in a dry nitrogen stream at 214°C. After different reaction times, the samples were cut into thin slices. The M_w profile within the sample was obtained through intrinsic viscosity measurements in a phenol–TCE mixture. At each location inside the sample, the $[\eta]$ vs. time curve typically shows a maximum, which is rather broad at the midplane and much sharper at the external surface. The phenomenon was mathematically described by accounting for both diffusion and chemical reactions within the slab; five simultaneous chemical reactions have been considered. The observed behavior is found to be essentially due to two competing processes, i.e., the diffusion of the low molecular weight species generated during the polycondensation and the thermal degradation reaction. The model predictions are compared with the experimental data showing a satisfactory agreement.

INTRODUCTION

Solid state postpolycondensation is a widely used procedure to increase the average molecular weight of polyesters and polyamides. The process is particularly important to achieve large values of M_w in the case of highly cristalline polymers with high melting temperature, when thermal degradation dominates in the melt phase. Relevant examples are recognized in poly(ethylene terephthalate) (PET) and in poly(butylene terephthlate) (PBT).[1-9]

Typically the polymer is heated up to temperature ranges which enhance propagation reactions, usually up to 20–50°C below T_m, in order to avoid particle sticking; then the polymer is kept under vacuum or in an inert gas stream which strips out the volatile condensation products. The overall process kinetics are thus influenced by the rate of all the simultaneous reactions and by the rate of diffusion of the low molecular weight compounds. So far a comprehensive quantitative description, which accounts for all the simultaneous kinetic steps, is still demanded.

In the case of PBT here considered, postpolymerization was previously studied in fine polymer particles so that the effects of diffusion were disregarded.[5,6,8]

Several chemical reactions can occur in the usual operating conditions, but only for a few of them are detailed studies available and a general consensus was achieved about their kinetics; for other reactions, on the other hand, either there is no universal agreement on the relevant kinetic

Journal of Applied Polymer Science, Vol. 29, 2873–2887 (1984)
 CCC 0021-8995/84/092873-15$04.00

mechanisms, or little attention has been payed to a quantitative kinetic description.

One of the main aims of a postpolycondensation analysis is to describe the local time change of the molecular weight and its relationships with operating conditions (temperature, sample thickness) and with initial conditions (hydroxyl to carbonyl end-group ratio and molecular weight). A satisfactory mathematical description is so far demanded in order to give a quantitative insight of the significant rate mechanisms and also to be able to describe the solid-state polycondensation in manufactured products as well as in fine powders.

In the present work we experimentally considered solid-state postpolymerization in thick PBT sheets from which M_w was measured vs. time at different specimen depths. A mathematical model was then constructed to describe the data, which accounts for diffusion of volatile products such as water, 1,4-butanediol (BD), and terephthalic acid and also accounts for as many as five chemical reactions. The values used for the kinetic constants were taken from literature data and were not treated as adjustable parameters. The specific effect produced by each reaction is also investigated and discussed.

Experimental

Materials and Samples. Poly(butylene terephthalate) specimens were obtained by injection moulding in sheets 3.15 $\pm$ 0.03 mm thick; the actual form is that required by ASTM D 638/I for tensile testing. The starting PBT polymer was obtained from dimethylphthalate (DMT) and 1,4-butanediol (BD), by using titanium tetrabutylate as catalyst; the initial catalyst to DMT weight ratio was 5.2×10^{-4}. The initial PBT used is characterized by intrinsic viscosity $[\eta] = 0.77$ dl/g, measured at 30°C in a phenol/tetrachloroethane solution, hydroxyl end-groups concentration 94 meq/kg, and carboxyl end-groups concentration 32 meq/kg.

Solid-state polycondensation was obtained by curing the samples in a stream of dry nitrogen at constant temperature; the apparatus used is shown in Figure 1. Temperature control is obtained by circulating silicon oil in the apparatus. The specimen surface temperature was measured through a thermocouple and was 214°C at the midpoint, while it was 212°C and 216°C, respectively, at points *a* and *b* (Fig. 1).

The nitrogen stream was first dried with molecular sieves, Merck 5 Å, then preheated at about 220°C; the nitrogen average velocity was kept constant at 0.3 m/s on the specimen surface throughout all postpolymerization runs.

After each solid-state polycondensation run, the specimens were left to cool down at room temperature in the air. Portions of polymer, 1.5 mm in depth, were removed from the small lateral surfaces of the specimens in order to exclude edge effects and to account only for a 1-dimensional diffusion process, in the direction perpendicular to the main surfaces of the specimen.

A milling cutter, with $\pm$0.02 mm precision, was then used to obtain thin slices corresponding to different depths in the slab. From the half-thickness of each specimen we thus obtained 10 samples, 0.15 mm thick; only the

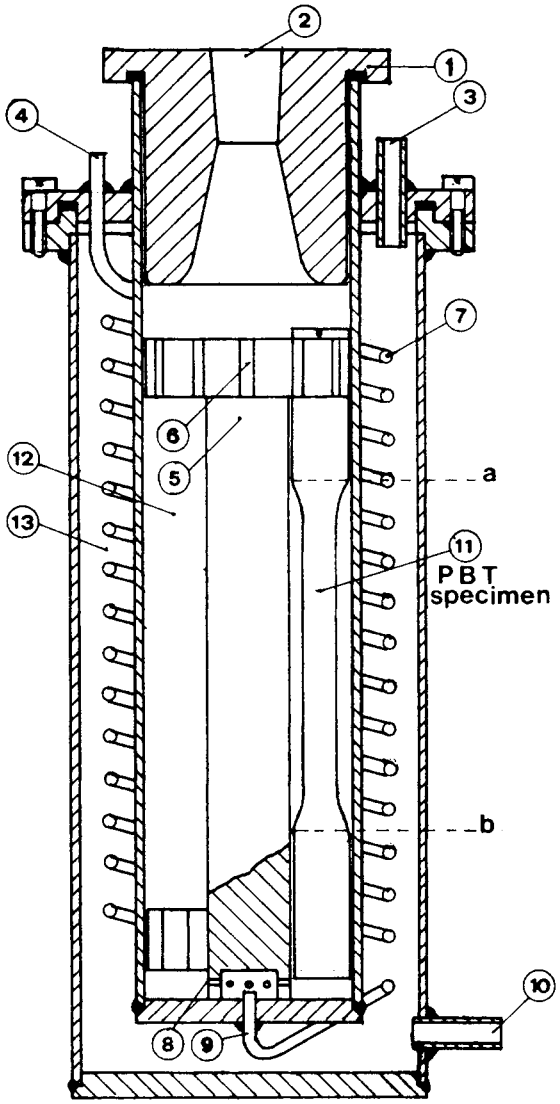

Fig. 1. Apparatus used for solid-state polycondensation: (1) teflon plug; (2) nitrogen outlet; (3) silicon-oil outlet; (4) nitrogen inlet; (5) specimen holder; (6) slats; (7) copper tube coil; (8) holes for distributing the gas evenly; (9) nitrogen inlet into the solid-state polycondensation room; (10) silicon–oil inlet; (11) PBT specimen; (12) solid-state polycondensation room; (13) silicon–oil bath.

portion a–b (see Fig. 1) of the original slab was used for this purpose. The thin slices obtained were used for intrinsic viscosity measurements.

Viscosity Measurements. Mixtures of 1,1,2,2-tetrachloroethane 40% by weight in phenol were used to dissolve polymer samples. Viscosity measurements were performed through Ubbelhode viscometers at 30.0 ± 0.02°C. All times measured are taken to within ± 0.02 s and are always longer than 100 s. The intrinsic viscosity was obtained for each sample from four solutions at different concentrations.

End-Groups Measurements. Carboxyl and total (carboxyl plus hydrox-

yl) end-group concentrations were measured as previously reported in Refs. 8 and 10.

Density Measurements. Densities were measured by the flotation method in carbon tetrachloride/*n*-hexane systems. It was observed that density remains constant through the specimen to within ± 0.002 g/cm^3, while it undergoes only slight changes with the duration of solid-state polycondensation, e.g., it changes from 1.315 to 1.323 g/cm^3 in 96 h. The degree of crystallinity, as weight fraction, was then calculated on the basis of the average density value of 1.319 g/cm^3, taken as a constant for all samples.

EXPERIMENTAL RESULTS

The intrinsic viscosity vs. polycondensation time is shown in Figure 2 for different locations inside the PBT specimen; in particular, we report the data for the midplane slice, for the surface slice, and for an intermediate slice located halfway between the center and the surface. The data shown are average values between several data points. A satisfactory reproducibility of the data was observed after differences in the injection moulding process or in the slicing procedure.

Intrinsic viscosity, and thus M_w shows at any sample depths the same qualitative progression during reaction time: a rather pronounced initial increase occurring in the first 20 h is then substantially reduced in the following 25 h; finally, the curves level off to near asymptotic values. The time at which the maximum value of M_w is obtained is roughly the same for all the locations inside the specimen, around 20 h, while the absolute values are rather different. Apparently, the increasing rate of M_w at the surface layer is much higher than it is in the two other locations for the entire period up to the time the maximum value is reached. Such a difference between outer and inner layers cannot be attributed to the thermal gradients which exist at early times; they will be significant only for periods

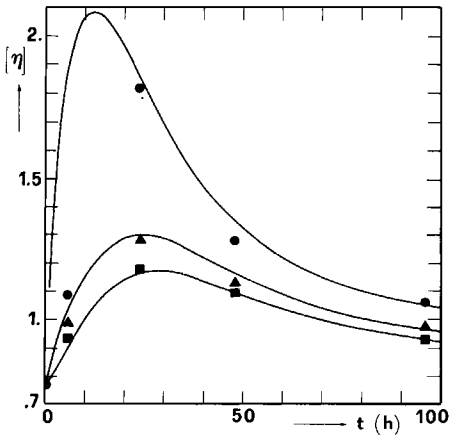

Fig. 2. Intrinsic viscosity vs. time in three sample slices: (■) central, $0 \leqslant \xi \leqslant 0.1$; (▲) intermediate, $0.5 \leqslant \xi \leqslant 0.6$; (●) surface, $0.9 \leqslant \xi \leqslant 1$. Comparison between model predictions (continuous line) and experimental data points.

of time of the order of 1 s, as can be estimated through the characteristic time for heat conduction, $t_c = \delta^2/a$; here δ is the sample semithickness and a indicates thermal diffusivity.

On the other hand, since outward diffusion of volatile condensation products is rather faster from the outer surface than from internal locations, we conclude that, at the initial stages, the solid-state polycondensation is a highly diffusion controlled process.

After the maximum M_w value has been reached, the M_w rate of decrease is again much larger for the external layer than for the internal ones. The above observation is consistent with the fact that polycondensation reactions are reversible and produce longer polymer chains simultaneously with low molecular weight condensation products. As long as polycondensation takes place in the internal core, the volatile products diffuse outward; thus, upon crossing the outer layers, they drive the reaction toward lower molecular weight polymers.

Figure 2 shows that at long times the molecular weight profile finally attains a nearly steady state value inside the sample and is higher at the surface and lower at the midplane; such a profile can be kept constant when a "dynamic" equilibrium is achieved between degradation and condensation reactions and outward diffusion of volatile species.

THEORY

Chemical Reactions and Their Kinetics

Let us consider here the main chemical reactions which can take place during PBT postpolycondensation. They can be schematically summarized as follows:

(i) Transesterification Reaction.

$$P_n \sim COO(CH_2)_4 \sim OH + HO \sim (CH_2)_4\,OOC \sim P_m \overset{k_1}{\rightleftharpoons} P_n \sim COO(CH_2)_4\,OOC \sim P_m + HO(CH_2)_4OH$$

By indicating by Y and E a hydroxyl polymer end group and an internal ester bond, respectively, the reaction will be synthetized as

$$Y + Y \overset{k_1}{\rightleftharpoons} E + G \tag{1}$$

where G indicates the volatile compound 1,4-butanediol.

As is widely recognized, the reaction is one of the most important during the melt polymerization of DMT and BD to PBT. It is an equilibrium reaction with equilibrium constant $K_1 = 0.4$.[11-13]

It is well known that reaction (1) is significant only in the presence of catalysts; it is catalyzed both by titanium alcoxide and by carboxyl end groups.[14] The former catalyst is much more effective than the latter one; thus we will consider reaction (1) as essentially titanium catalyzed. In both

cases, however, the forward reaction was found to be second order in the molar hydroxyl end-group concentration.[11,15] From studies of model molecules reactions[11,12] the overall kinetic constant k_1, already accounting for titanium alcoxide concentration, is evaluated to be 6.1×10^{-4} (L/mol · s) at 214°C.

(ii) Esterification Reaction.

$$P_n \sim COO(CH_2)_4 \sim OH + HOOC \sim P_m \overset{k_2}{\rightleftharpoons} P_n \sim COO(CH_2)OOC \sim P_m + H_2O$$

This reaction will be schematically referred to as:

$$Y + Z \overset{k_2}{\rightleftharpoons} E + W \tag{2}$$

where Z indicates the carboxyl end group and W stands for water. As is reaction (1), reaction (2) is also reversible and catalyzed by both titanium alcoxide and carboxyl end-groups[11,14].

Usually reaction (2) becomes relevant in late stages of polycondensation of DMT and BD, when the carboxyl end-group concentration becomes significant. In spite of the many studies about reaction (2), there is not a general agreement about its kinetic mechanism and about the partial orders of reaction with respect to Y and Z.[16] In many cases reaction (2) has been found to be first order in both carboxyl and hydroxyl end-group molar concentration.[11,16,17] That will also be our assumption. From previous studies on model molecules reactions[11,12] the overall kinetic constant k_2, already accounting for titanium alcoxide concentration, is evaluated to be 7.6×10^{-4} (L/mol s) at 214°C. The equilibrium constant is reported to be $K_{2q} = 1$.[17]

(iii) Degradation Reaction.

$$P_n \sim COO(CH_2)_4\,OOC \sim P_m \xrightarrow{k_3} P_n \sim COOH + P_m \sim COOH + CH_2{=}CH{-}CH{=}CH_2$$

Synthetically it will be referred to as

$$E \xrightarrow{k_3} Z + Z \tag{3}$$

The presence of 1,3-butadiene is dropped in the short-hand notation since its presence is recognized to be ineffective in view of the irreversibility of the reaction. It is the main chain cleavage reaction in our system. Its kinetic mechanism is well known and leads to a rate law which is first order in the molar concentration of ester bonds[18–20]; values of the kinetic constant k_3 were obtained from both PBT and model molecules studies and are reported in Refs. 18–20.

(iv) Side Reaction.

$$P_n \sim COO(CH_2)_4\,OH \xrightarrow{k_4} P_n \sim COOH + THF$$

Synthetically it will be referred to as

$$Y \xrightarrow{k_4} Z \tag{4}$$

and the presence of tetrahydrofuran (THF) will not be explicitly considered in view of the irreversibility of the reaction.

Although reaction (4) has no direct effect on the molecular weight, it can play a significant role insofar as it changes hydroxyl into carboxyl end groups. Its kinetics have been already studied[20] and proved to be unaffected by both titanium alcoxide and carboxyl groups. The reaction is first order in Y molar concentration; values of the kinetic constant have been reported in Ref. 20.

(v) Acidolysis.

$$P_n \sim COO(CH_2)_4\,OOC \sim P_m + HOOC \sim P_r \overset{k_5}{\rightleftharpoons} HOOC \sim P_m + P_n \sim COO(CH_2)_4OOC \sim P_r$$

It represents an equilibrium interchange reaction; it can be effective on the molecular weight increase, when a rather volatile product is obtained. Actually, the presence of terephthalic acid has been repeatedly recognized in the gas stream during either melt polymerization or solid-state postpolycondensation.[8] In what follows, the above reaction will be accounted for only in the particular case in which P_m–COOH is the terephthalic acid, shortened as V. In our synthetic notation the reaction will be referred to as:

$$Z + Z \overset{k_5}{\rightleftharpoons} E + V \tag{5}$$

Apparently, no kinetic information is available for the above reaction in systems like PBT, PET, or their models. As far as we can learn, we can nonetheless benefit from kinetic data for the acidolysis reaction in polycarbonates, as reported in Ref. 21, as soon as we consider the reactivity of ester groups similar to that of carbonate groups. From Ref. 21, reaction (5) was considered to be second order in the molar concentration of Z; the kinetic constant k_5 has a preexponential factor of 2.37×10^{10} cm^3/(mol · min) and an activation energy of 23.4 kcal/mol. As far as the equilibrium constant is concerned, the reasonable assumption was made that $K_5 = 1$.[22]

(vi) Alcoholysis.

$$P_n \sim COO(CH_2)_4OOC \sim P_m + HO(CH_2)_4OOC \sim P_r \rightleftharpoons P_n \sim COO(CH_2)_4OOC \sim P_r + HO(CH_2)_4OOC \sim P_m$$

(vii) Esterolysis.

$$P_n \sim COO(CH_2)_4OOC \sim P_m + P_s \sim COO(CH_2)_4OOC \sim P_r \rightleftharpoons$$
$$P_n \sim COO(CH_2)_4\,OOC \sim P_s + P_m \sim COO(CH_2)_4OOC \sim P_r$$

As well as reaction (v), both reactions (vi) and (vii) are equilibrium interchange reactions which can be effective on M_w changes as long as low volatility products are formed, which can be subtracted from the system in significant amounts. The volatility of the oligomers originated through reactions (vi) and (vii) is usually rather small when compared with that of the other volatile compounds previously considered. It is worth noticing, in addition, that intramolecular reactions as (vi) and (vii) can also lead to the formation of volatile cyclic oligomers, which have actually been recognized in the vapour products. Nonetheless, the M_w changes which are obtained from their stripping are not appreciable. Therefore, we feel confident that neglecting both (vi) and (vii) reactions will result in nothing else but negligible effects on M_w and on $[\eta]$.

In what follows we will consider the reaction system including only reactions (1)–(5). In view of the high differences in mobility, the reactions will be assumed to take place only in the amorphous region and not in the crystalline phase. In addition, all end groups and Ti compounds are considered to be present in the amorphous region only.

The degree of crystallinity of PBT samples was measured, as usual, through density data. The density of the amorphous phase, extrapolated after van Krevelen and Hftyzer[23] from the value of 1.278 g/cm^3 at 25°C,[24] is estimated to be $\rho_a = 1.154$ g/cm^3 at 214°C. By using $\rho_c = 1.397$ g/cm^3 as the density of the perfectly crystalline region,[25] the crystallinity, X_{cw}, was obtained in our starting PBT as 36% by weight.

As reported above, one can find the values of the kinetic constants from reported data either in melt or in model solution reactions. Although the reactive group mobility in the amorphous phase might not be precisely equal to that in the melt or in solutions, it is nonetheless expected to have rather close values in all cases. Our first guess will thus be to consider the kinetic constants as values already known from the literature and not adjustable parameters.

Balance Equations and Mathematical Model

The mathematical description of the postpolycondensation process of PBT is obtained by writing down the balance equations for species Y,Z,G,W and V; their concentration, indicated by y,z,g,w, and v, respectively, are functions of the reaction time t and of the spatial position x. The only diffusing species are G, W, and V, and thus the following set of mixed first and second order partial differential equations is obtained:

$$\frac{\partial y}{\partial t} = -2k_1y^2 + 2\frac{k_1e}{K_1}g - k_2yz + \frac{k_2e}{K_2}w - k_4y \tag{6}$$

$$\frac{\partial z}{\partial t} = -k_2 yz + \frac{k_2 e}{K_2} w + 2\, k_3 e + k_4 y - 2k_5 z^2 + 2\frac{k_5 e}{K_5} v \tag{7}$$

$$\frac{\partial g}{\partial t} = \frac{\mathscr{D}_G}{\delta^2}\frac{\partial^2 g}{\partial \xi^2} + k_1 y^2 - \frac{k_1 e}{K_1} g \tag{8}$$

$$\frac{\partial w}{\partial t} = \frac{\mathscr{D}_W}{\delta^2}\frac{\partial^2 w}{\partial \xi^2} + k_2 yz - \frac{k_2 e}{K_2} w \tag{9}$$

$$\frac{\partial v}{\partial t} = \frac{\mathscr{D}_V}{\delta^2}\frac{\partial^2 v}{\partial \xi^2} + k_5 z^2 - \frac{k_5 e}{K_5} v \tag{10}$$

The symbol $\mathscr{D}_i$ represents the diffusion coefficients of species i; ξ indicates the dimensionless spatial position within the specimen, perpendicular to the main outer face, $\xi = x/\delta$; at the midplane $\xi = 0$ while at the outer surface $x = \delta$ and $\xi = 1$.

The initial and boundary conditions for the problem are given as follows:

$$\text{IC: } y(\xi,0) = y_0,\ z(\xi,0) = z_0,\ g(\xi,0) = w(\xi,0) = v(\xi,0) = 0 \tag{11}$$

$$\text{BC 1: } \xi = 0, \forall t \geqslant 0,\ \frac{\partial g}{\partial \xi} = \frac{\partial w}{\partial \xi} = \frac{\partial v}{\partial \xi} = 0 \tag{12}$$

$$\text{BC 2: } \xi = 1, \forall t \geqslant 0,\ g = w = v = 0 \tag{13}$$

In the initial conditions the volatile components were considered not to be present, in the absence of precise experimental informations; it is to be observed, however, that at low temperatures, when all reactions are ineffective, such species had most likely diffused out of the samples. In any case the above assumption will affect only the early stages of the process.

The boundary conditions used at the outer surface, BC 2, is actually consistent with the fact that the mass transfer resistance is here totally dominated by the diffusion within the solid; in fact the order of magnitude of the Biot number, $\text{Bi} = K_c\delta/\mathscr{D}$ with K_c outer mass transfer coefficient, can be easily estimated to be well above 1000.

The reactions are considered to take place in the amorphous phase only; the concentration of the ester bonds is assumed to be constant and equal to 10.49 mol/L.

Equations (6)–(10) with conditions (11)–(13) were solved numerically by using an implicit Crank–Nicholson procedure in order to achieve numerical stability; a linearized system was adopted. The numerical procedure is reported in some detail in Appendix A.

The mathematical model gives for any spatial position the time dependence of hydroxyl and carboxyl end-group concentrations, as well as that of the volatile products considered. From the above data the number-average molecular weight M_n is calculated as follows:

$$M_n = \frac{1000\ \rho_a}{\frac{1}{2}(y + z)(1 - X_{cw})} \tag{14}$$

M_w is then calculated by assuming that the most probable molecular weight distribution holds true locally; i.e., at any x we have

$$M_w = 2M_n - M_0 \tag{15}$$

where M_0 is the repeating unit molecular weight.

A power low relationship is then used to correlate M_w to $[\eta]$ values:

$$[\eta] = KM_w^a \tag{16}$$

In our case the values of $K = 9.31 \times 10^{-5}$ dL/g and $a = 0.871$ were used.[26]

MODEL RESULTS AND DISCUSSION

Since the experimental data reported above refer to values obtained from slices 0.15 mm thick and not to point values, the model results were suitably averaged over the corresponding slices of the sample in order to adequately compare model predictions with the average experimental data.

From the mathematical point of view the model contains 11 parameters, namely, three equilibrium constants K_1, K_2, and K_5, five kinetic constants k_1–k_5 and three diffusion coefficients $\mathscr{D}_W$, $\mathscr{D}_G$, and $\mathscr{D}_V$. The equilibrium and the kinetic constants, however, are known from the literature, although under conditions different from the ones of interest here. For such quantities, however, we used exactly the values obtained by interpolating or extrapolating literature data; those values are summarized in Table I.

Only the diffusion coefficients were thus used as parameters, although their orders of magnitude are already known in advance from similar physical systems (e.g., Refs. 27–29).

Figure 2 shows the predicted time progression of $[\eta]$ for three slices.

Experimental data are also reported for direct comparison. The calculations were performed by using the following diffusion coefficients:

$$\mathscr{D}_G = 10^{-5}\ \text{cm}^2/\text{s},\ \mathscr{D}_W = 1.2 \times 10^{-5}\ \text{cm}^2/\text{s},\ \mathscr{D}_V = 4 \times 10^{-6}\ \text{cm}^2/\text{s}$$

For the same parameter values, Figure 3 shows the internal $[\eta]$ profile at different reaction times.

TABLE I
Kinetic and Equilibrium Data for the Relevant Chemical Reactions Entering the Model

	Reaction	Eq. Constant	Kin. Constant	Ref.
1	$Y+Y \rightleftharpoons E+G$	0.4	6.1×10^{-4} L/mol·s	11,12
2	$Y+Z \rightleftharpoons E+W$	1.0	7.6×10^{-4} L/mol·s	11,12
3	$E \longrightarrow Z+Z$	—	$3.5 \times 10^{-8}\ s^{-1}$	18,20
4	$Y \longrightarrow Z$	—	$0.9 \times 10^{-5}\ s^{-1}$	20
5	$Z+Z \rightleftharpoons E+V$	1.0	1.25×10^{-5} L/mol·s	21

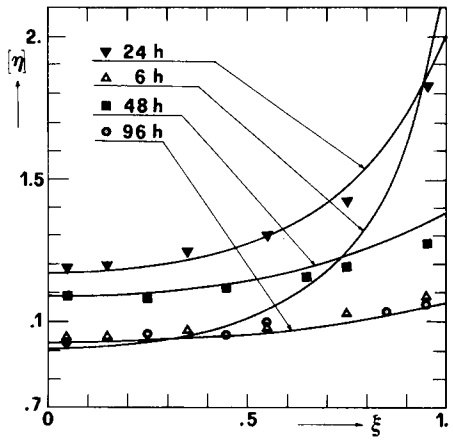

Fig. 3. Intrinsic viscosity profiles at various reaction times; comparison between model predictions (continuous line) and experimental data points.

As is apparent, the model predictions are in a quite satisfactory agreement with the experimental data at all times and spatial positions. A remarkable deviation from the experimental datum, however, is given at the early stages for the surface layer. A reasonable explanation for that could be found in the possible initial structure differences which exist between surface and internal layers, such as skin-core structure as reported in Ref. 30 for injection-molded PBT.

In the absence of a broad set of experimental data, no parameter optimization technique was applied to obtain optimal values. In spite of that, it is rather surprising and encouraging to find that the model predictions fit quite nicely the experimental behavior by using reasonable values for the diffusion coefficients and only literature data for the reaction rate and equilibrium constants.

Some comments are now in order about the relative importance of the physical mechanisms accounted for.

The initial postpolycondensation period, roughly up to the time t_{max} at which the maximum value of $[\eta]$ is reached, is dominated by the condensation reactions (1) and (2) in competition with the degradation reaction (3); when acidolysis reaction (5) is disregarded, in fact, almost the same $[\eta]$ profiles are initially obtained.

As is apparent from the sharp $[\eta]$ gradient at the outer surface, the condensation reactions (1) and (2) are diffusion controlled and they are thus very close to equilibrium. They are competitive reactions; the rate of reaction (1) suddenly decreases in the early stages of the process; indeed it is of second order in hydroxyl end groups, which rapidly disappear due to reactions (1), (2), and (4). Reaction (2), on the contrary, is important up to t_{max}, due to the increasing Z concentration (Fig. 4).

The maximum value of $[\eta]$ is thus greatly dependent on water diffusivity, $\mathscr{D}_W$, which controls the reaction (2).

The diffusivity of butanediol, $\mathscr{D}_G$, as well as the kinetic constant k_1, are not such critical parameters in determining the maximum value of $[\eta]$; a

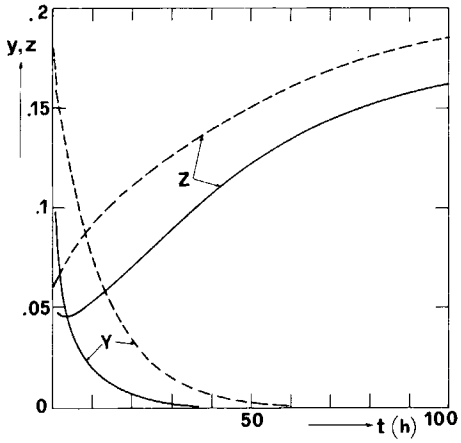

Fig. 4. Model predictions for hydroxyl, Y, and carboxyl, Z, end-groups concentration vs. time: (——) values in the surface slice; (···) values in the midplane slice.

decrease in k_1 or $\mathscr{D}_G$ values only slightly increases t_{max} and the maximum of $[\eta]$.

That behavior can be easily understood by observing that the same chain length increase is obtained through the consumption of two hydroxyl end groups in reaction (1) while only one is needed in reaction (2); if reaction (1) is slowed down, then reaction (2) can be effective for longer times.

At about the time t_{max}, the hydroxyl end groups have almost completely disappeared in the surface slice (Fig. 4); a sudden decrease in molecular weight is then produced by the thermal degradation (3). The slope in the $[\eta]$ vs. time curve soon after the maximum is largely given by the degradation rate constant k_3.

At long times the competition between degradation and the acidolysis reaction (5) dominates the overall kinetics.

Reaction (5) is a reversible reaction, but is not diffusion-controlled as reactions (1) and (2); actually both chemical kinetics and diffusion influence the overall rate of reaction (5).

It is worthwhile pointing out that usually reaction (5) is not included among the relevant reactions for PBT postpolycondensation. In that case a continuous and marked decrease in $[\eta]$ would always be obtained at long times, contrary to our experimental observation of a nearly asymptotic behavior. Actually, previous experimental data analyzed only the initial postpolycondensation times at which the influence of reaction (5) is not clearly apparent.

Finally we observed that changes in the initial concentrations of BD, water, and terephthalic acid from zero to the equilibrium values do not affect at all the observed behaviors.

CONCLUSIONS

Postpolycondensation of PBT can be successfully modeled taking into account five chemical reactions and the diffusion of three volatile species. The molecular weight increases and reaches a maximum, after which ther-

mal degradation prevails. At longer times an asymptotic value is reached due to the acidolysis reaction (5), in competition with thermal degradation.

Up to the maximum, the process is dominated by the transesterification reaction (1) and by the esterification reaction (2); in our experimental conditions both were diffusion controlled. Reaction (2) was found to be more effective to an M_w increase; the maximum value of molecular weight strongly depends on the water diffusivity.

The authors are indebted to Montepolimeri Research Center Giulio Natta, Ferrara, for supplying the specimens. The authors wish to thank Mr. A. Scagliarini for his help in the experimental work.

APPENDIX A: LINEARIZATION AND INTEGRATION OF THE EQUATIONS

The system at hand is

$$\frac{\partial \mathbf{Y}}{\partial t} = \frac{\partial^2 \mathbf{Y}}{\partial x^2} + \mathbf{R}(\mathbf{Y}), \quad 0 \leqslant x \leqslant 1 \tag{17}$$

where the generation vector $\mathbf{R}$ is a nonlinear function of the concentration vector $\mathbf{Y}$. The Crank–Nicholson method leads to the following set of algebraic equations:

$$\left(\frac{\Delta \mathbf{Y}}{\Delta t}\right)_i = \frac{1}{2}\left[\left(\frac{\Delta^2 \mathbf{Y}}{\Delta x^2}\right)_j + \left(\frac{\Delta^2 \mathbf{Y}}{\Delta x^2}\right)_{j+1}\right] + \mathbf{R}_{j+1/2} \tag{18}$$

where i and j label the descrete space and time positions, respectively. Though the grid points i are usually equally spaced, in our case a thinner grid was preferred close to the surface $x = 1$. To that purpose a constant reduction ratio $\alpha = \Delta x_i / \Delta x_{i-1}$ was used; the second-order finite difference was calculated by using a parabolic interpolation as

$$\left(\frac{\Delta^2 \mathbf{Y}}{\Delta x^2}\right)_i = \frac{2\alpha}{\alpha + 1} \frac{\alpha \mathbf{Y}_{i-1} - (\alpha + 1)\mathbf{Y}_i + \mathbf{Y}_{i+1}}{(\Delta x_1)^2 \, \alpha^{2(i-1)}} \tag{19}$$

In our case the nonlinearity in $\mathbf{R}(\mathbf{Y})$ is only due to quadratic terms as $\mathbf{Y}_k \mathbf{Y}_l$. We took advantage of that to obtain linear algebraic equations, since

$$(\mathbf{Y}_k \mathbf{Y}_l)_{j+1/2} \simeq \frac{\mathbf{Y}_{kj} \mathbf{Y}_{l,j+1} + \mathbf{Y}_{k,j+1} \mathbf{Y}_{l,j}}{2} \tag{20}$$

It can be shown that, to within terms of the order of $\Delta \mathbf{Y}_k \cdot \Delta \mathbf{Y}_l$, the rhs of eq. (20) is equal to both the mean value between $(\mathbf{Y}_k \mathbf{Y}_l)_j$ and $(\mathbf{Y}_k \mathbf{Y}_l)_{j+1}$ as well as to the product of the mean $\mathbf{Y}_k$ and $\mathbf{Y}_l$ values. When $k = l$ eq. (20) reduces to the geometric mean.

According to the above method, the integration of eqs. (6)–(10) requires the solution of $5M + 2$ linear algebraic equations at each time step, M being the number of the spatial grid intervals. The matrix of the coefficients has the structure shown in Fig. 5.

The solution was obtained in two steps: triangularization and back substitution. The computation time was minimized taking advantage of the matrix sparsity both in triangularization and back substitution steps. Accurate results were obtained with $M = 20$, $\alpha = 0.9$, and $\Delta t = 5$ min.

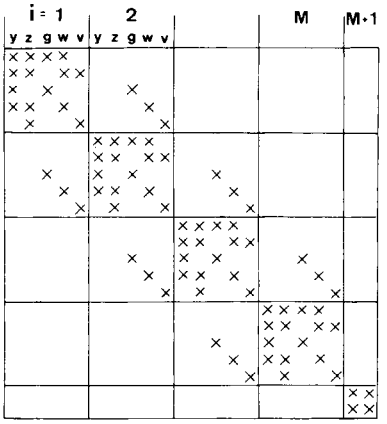

Fig. 5. The structure of the coefficient matrix for the system to be solved at each time step. Every block of five rows represents the five mass balance equations at the point *i*.

APPENDIX B: NOMENCLATURE

BD = G 1,4-butanediol
$\mathscr{D}$ diffusion constant
E ester bond internal to PBT chains
K equilibrium constant
k kinetic constant
T_m melting temperature
V terephthalic acid
W water
X_{cw} crystallinity weight fraction
Y hydroxyl end group
Z carboxyl end group
e,g,v,z,y,w concentrations (mol/L) referring to the amorphous phase
δ specimen semithickness
ξ dimensionless axial position
$[\eta]$ intrinsic viscosity

References

1. Li-Chen Hsu, *J. Macromol. Sci. Phys. B1*, **4**, 801 (1967).
2. F. C. Chen, R. G. Griskey, and G. H. Beyer, *AIChE J.*, **15**, 680 (1969).
3. T. M. Chang, *Polym. Eng. Sci.*, **10**(6), 364 (1970).
4. M. Dröscher and G. Wegner, *Polymer*, **19**, 43 (1978).
5. L. H. Buxbaum, *J. Appl. Polym. Sci., Appl. Polym. Symp.*, **35**, 59 1979).
6. H. D. Dinse and E. Tucek, *Acta Polym.*, **31**, 108 (1980).
7. E. Schaaf, H. Zimmermann, W. Dietzel, and P. Lohmann, *Acta Polym.*, **32**, 250 (1981).
8. B. Fortunato, F. Pilati, and P. Manaresi, *Polymer*, **22**, 655 (1981).
9. S. Chang, M.-F. Shen, and S. M. Chen, *J. Appl. Polym. Sci.*, **28**, 3289 (1983).
10. W. H. F. Borman, *J. Appl. Polym. Sci.*, **22**, 2119 (1978).
11. F. Pilati, P. Manaresi, B. Fortunato, A. Munari, and P. Monari, *Polymer*, **24**, 1479, (1983).
12. F. Pilati, P. Manaresi, A. Munari, and V. Bonora, Short communication and posters, AIM, 6° Convegno Italiano di Scienza e Tecnologia delle Macromolecole, Pisa, 10–14 October 1983, p. 393.
13. G. Challa, *Makromol. Chem.*, **38**, 105 (1960).
14. F. Pilati, P. Manaresi, B. Fortunato, A. Munari, and V. Passalacqua, *Polymer*, **22**, 799 (1981).

15. B. H. Bamford and C. F. H. Tipper, *Comprehensive Chemical Kinetics—Non Radical Polymerization*, Elsevier, Amsterdam, 1976, Vol. 15.
16. A. Fradet and E. Marechal, *Adv. Polym. Sci.*, **43**, 51 (1982).
17. I. Goodman, in *Encyclopedia of Polymer Science and Technology*, H. F. Mark and N. G. Gaylord, Wiley-Interscience, New York, 1976, Vol. 11, p. 92.
18. V. Passalacqua, F. Pilati, V. Zamboni, B. Fortunato, and P. Manaresi, *Polymer*, **17**, 1044 (1976).
19. J. Devaux, P. Godard, and J. P. Mercier, *Macromol. Chem.*, **179**, 2201 (1978).
20. F. Pilati, P. Manaresi, B. Fortunato, A. Munari, and V. Passalacqua, *Polymer*, **22**, 1566 (1981).
21. J. Devaux, P. Godard, and J. P. Mercier, *Polym. Eng. Sci.*, **22**, 229 (1982).
22. E. W. Eckey and E. F. Izard, in *Encyclopedia of Chemical Technology*, Kirk-Othmer, Wiley-Interscience, New York, 1965, Vol. 8, p. 361.
23. D. W. Van Krevelen and P. J. Hftyzer, *Properties of Polymers*, Elsevier, Amsterdam, 1976.
24. S. J. Hobbs and C. F. Pratt, *J. Appl. Polym. Sci.*, **19**, 1701 (1975).
25. I. J. Desborough and I. H. Hall, *Polymer*, **18**, 825 (1977).
26. F. Pilati, A. Munari, and P. Manaresi, *Mat. Chem.*, **7**, 649 (1982).
27. J. S. Vrentas and J. L. Duda, *AIChE J.*, **25**, 1 (1979).
28. T. M. Pell Jr. and T. G. Davis, *J. Polym. Sci., Polym. Phys. Ed.*, **11**, 1671 (1973).
29. G. Rafler, E. Bonatz, G. Reinish, I. Ruhnau, H. Gajewski, and H. D. Sparing, *Acta Polym.*, **34**, 48 (1983).
30. S. Y. Hobbs and C. F. Pratt, *J. Appl. Polym. Sci.*, **19**, 1701 (1975).

Received December 23, 1983
Accepted January 16, 1984